

# An Extended Tension Leg Platform Design for Post-Katrina Gulf of Mexico

John Murray, Chan K. Yang and Wooseuk Yang  
FloaTEC, LLC Houston, Texas

Partha Krishnaswamy,  
J. Ray McDermott, Houston, Texas

Jun Zou  
Houston Offshore Engineering, Houston, Texas

## ABSTRACT

The new metocean criteria for the Gulf of Mexico (GoM) affect changes to existing design procedures for future and existing offshore platform designs in that region. FloaTEC, LLC is completing the pre-FEED design on a version of its extended tension leg platform (ETLP) for deployment in this new environment at a water depth of 5,000 ft. This new GoM design was tested at a model scale of 1:92 under the new metocean criteria and instrumented to measure extreme responses, including wave runup, airgap tendon tensions, and six-degree-of-freedom motions. The paper presents and discusses the results of the predictions from an uncoupled and fully coupled model in comparison to the measured test data.

**KEY WORDS:** Extended Draft Tension Leg Platform; uncoupled and coupled model; Scaled model tests; Post-Katrina Gulf of Mexico conditions.

## NOMENCLATURE

$M$  : system mass matrix,  
 $M_{UC}$  : equivalent constant mass matrix modeling tendon effect,  
 $K$  : system stiffness matrix (hydrostatic),  
 $K_{UC}$  : equivalent constant stiffness matrix for tendon and riser effect,  
 $C$  : equivalent linear damping matrix to model the viscous damping,  
 $M^a(\infty)$  : equivalent added mass of the body at infinite frequency,  
 $F_i(t) = F_i^{(1)}(t) + F_i^{(2)}(t)$  : first and second-order wave excitation,  
 $F_R(\dot{x}, t) = -\int R(t-\tau)\dot{x}d\tau$  : radiation damping force,  
 $R(t) = \frac{2}{\pi} \int_0^\infty C(\omega) \frac{\sin \omega t}{\omega} d\omega$  : retardation function damping coefficient,  
 $F_{wind}(t)$  : wind force,  
 $F_m(\dot{x}, t) = \frac{1}{2} \rho C_D A (\underline{u}_n - \dot{x}_n) |\underline{u}_n - \dot{x}_n|$  : force on the Morison members,

$A$  : projected area of the Morison member,  
 $\underline{u}_n$  : particle velocity normal to the member (wave + current)  
 $\underline{\dot{u}}_n$  : particle acceleration normal to the member (wave + current)  
 $\dot{x}_n$  : velocity of the model element,  
 $K_C$  : time- and motion- dependent coupled stiffness matrix,  
 $F_C(\underline{x}, \dot{x}, \ddot{x}, t)$  : coupling tendon and riser force vector.  
 $w$  : weight of the model element per unit length,  
 $F^s$  : hydrostatic force on the model element per unit length,  
 $F^d$  : hydrodynamic force on the model element per unit length.

## INTRODUCTION

The new metocean criteria [API, 2007] for the Gulf of Mexico (GoM), brought on by the aftermath of recent hurricanes will affect changes to recommended design procedures for future and existing offshore platform designs in that region. The accuracy of the sizing tools and procedures used to predict the responses of floating systems become more stringent as a better understanding and quantification of the margins of conservatism take a critical role. In more practical terms, more accurate designs tools can identify the level of conservatism used in the original. This is useful in establishing whether the existing design is suitable for the newly defined criteria. Sizing tools for floating offshore structures are generally based on coupled [Kim et al, 1994] [Ran et al, 1997] or uncoupled [Oran, 1983] techniques. In some cases the uncoupled methods produce conservative quantities; however the converse can also be true.

FloaTEC, LLC is completing the pre-FEED design on a version of its Extended Tension Leg Platform (ETLP) for deployment in this new environment at a water depth of 5,000 ft.

The main feature of the ETLP design discussed later in this paper is extensions on the pontoon from which the structure derives its name.

The design tool used to size this hull and tendons involves a fully-coupled time domain solution incorporating top tensioned risers (TTRs), tendons, and the ETLP hull. This new ETLP design has undergone a model test program at a scale of 1:92 under the new GoM metocean criteria [API, 2007]. The test program included wind tunnel and wave tests. Data generated from the model tests are used to evaluate the design tool and to compare and discuss the predictions generated from an uncoupled model.

The Extended Tension Leg Platform (ETLP), illustrated in Fig. 1, consists of four columns connected underwater by four pontoons. The pontoon extensions move the tendon connection point outboard of the columns. The extensions effectively increase the restoring effect of the tendons while reducing the column spacing. This reduces the deck span between columns and thereby captures a saving in deck steel weight. The columns are circular for structural efficiency and to minimize environmental loading.

The structure is moored using 12 tendons; three tendons per corner, connected 18 ft above the keel. Principal prototype dimensions of the hull are given in Fig. 2 and listed in Table 1.

### UNCOUPLED AND FULLY COUPLED - EQUATIONS OF MOTION

The three typical methods of solution for the equations of motion of the TLP are frequency domain, uncoupled time domain, and coupled time

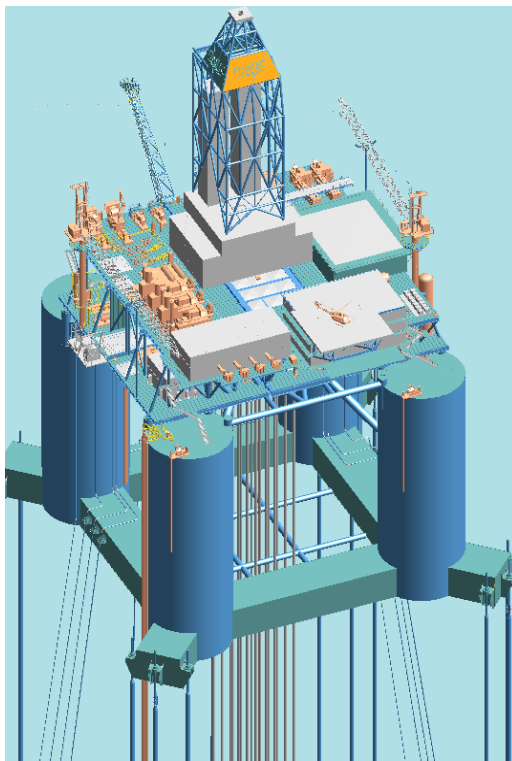


**Fig. 1 Extended Tension Leg Platform (ETLP)**

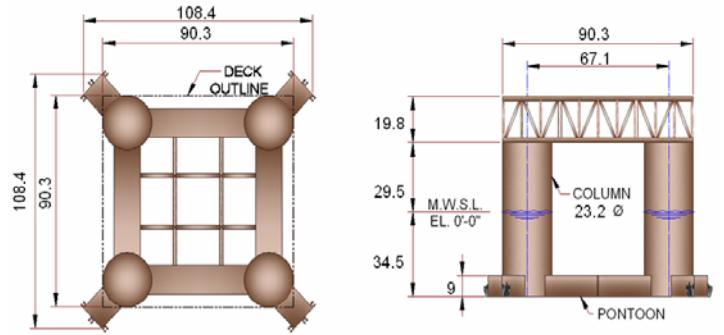


**Fig. 2 ETLP Configuration**

**Table 1 ETLP Specifications**

ETLP Particulars	
Displacement [Mt]	86,542.55
Tendon Pretension [Mt]	23,898.87
TTR Pretension [Mt]	5,886.97
Draft [m]	34.50
Free Board [m]	29.50
Column Diameter [m]	23.20
Column Height [m]	64.00
Pontoon Length [m]	43.86
Pontoon Width [m]	12.34
Pontoon Height [m]	9.00
Extended Pontoon Length [m]	11.50

domain. The equations of motion are the same in all methods, but their solution formulation reflects the limitations of the method selected.

The frequency domain analysis is the closed form solution of equations to estimate responses to random waves, including platform motions and accelerations, tendon loads and angles, and hydrodynamic loads. The most significant limitation of frequency domain techniques is that all nonlinearities in the equations of motion must be ignored or replaced by linear approximations. In cases where both time and frequency domain techniques are applicable, the frequency domain often has the advantage of simplifying the computations; so it is typically used for preliminary design since it can be used to estimate the short-term statistics of the variable of interest. However, the linearization required for frequency domain analysis might lead to inaccurate results for extreme loads.

Time domain analysis is the direct numerical integration of the equations of motion, allowing the inclusion of all system nonlinearities. Equation (1) describes the equation of motion for uncoupled analysis. All terms are defined in the nomenclature.

$$[M + M^a(\infty) + M_C] \ddot{x} + [C] \dot{x} + [K + K_C] x = F_I(t) + F_R(\dot{x}, t) + F_m(x, t) + F_{wind}(t) \quad (1)$$

The mass matrix term in Equation (1) shows a term  $M_C$ , which is an equivalent mass matrix term for the tendons and risers [Oran, 1983]. This represents a diagonal matrix for mass and added mass components in the horizontal and vertical directions. The stiffness matrix of the equation also shows a matrix of linearized stiffness constants,  $K_C$  [Garrett, 1982], to account for the riser and tendon reaction forces with the hull. This fully populated coefficient matrix is generated as a function of the ETLP offset from its still-water equilibrium position. Analyses with tendons and risers modeled in this method have no inertia or bending response. The forcing functions on the right hand side of the equation do not consider any environmental loads on the tendons or risers directly.

Equation (2) describes the equation of motion for the fully-coupled nonlinear model. All terms are defined in the nomenclature.

$$[M+M^*(\infty)]\ddot{x}+[K+K_C(x,t)]x=F_f(t)+F_R(\dot{x},t)+F_m(x,t)+F_{wind}(t)+F_C(x,\dot{x},\ddot{x},t) \quad (2)$$

The  $M_C$  term in the mass matrix is now part of the right hand side containing the forcing terms, expressed as  $F_C$ . The response of the tendons is calculated simultaneously with the platform response. Dynamic force interaction between the tendons and risers and platform at the points of attachment is included. The model includes dynamic tension and bending accounting for the nonlinearities in each riser and tendon as well as coupling effects. These effects are accounted for in the matrix  $K_C(x,t)$  which resolves the coefficients for each position using the finite-element model of the tendons and risers [Patel, 1983]. Thus, this matrix changes as a function of position and accounts for nonlinearities in the global restoring forces [Kim et al, 1994] [Ran et al, 1997].

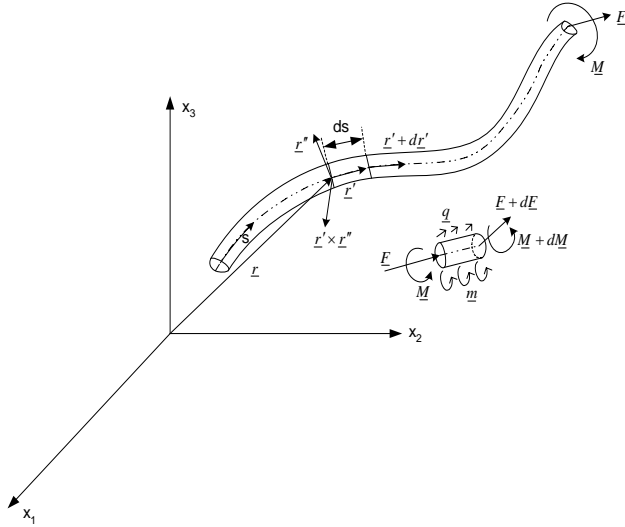


Fig. 3 Illustration of Slender Rod Model

Tendon loads consist of both static and dynamic components. Static loads arise from tendon pretension, tide, platform offset due to steady environmental forces and foundation installation position errors. These loads can be determined from the equilibrium conditions of the platform, tendons, and risers. Dynamic tendon loads arise from platform possible seismic induced motions, and direct hydrodynamic forces.

The forces on the tendons interacting with the hull are found using the technique illustrated in Fig. 3. The figure shows the configuration of a slender rod model and the free body diagram of forces and moments. The position vector  $\underline{r}(s,t)$  is a function of the arc length  $s$  of the rod at time  $t$ .  $\underline{F}$  and  $\underline{M}$  are the total resultant force and moment, respectively, acting on the rod cross section. The distributed load  $\underline{q}$  is divided per equation (3).

$$\underline{q} = \underline{w} + \underline{F}^s + \underline{F}^d \quad (3)$$

When a tendon or riser is free to move in wave and current, the independent flow field model is obtained by linear superposition of two independent flow fields; a far field due to the wave and current and a near field reacting to the structure motion.

The hydrodynamic force component on a tendon or riser is then

computed from equation (4).

$$\underline{F}^d = -C_A \rho A_I \ddot{x}_n + C_M \rho A_I \dot{u}_n + C_D \rho A_D |u_n - \dot{x}_n| (u_n - \dot{x}_n) \quad (4)$$

The total force on the member at time,  $t$ , is found by integrating along total length,  $S$ , as given in equation (5).

$$\underline{F}_C(x, \dot{x}, \ddot{x}, t) = \int \underline{q} ds \quad (5)$$

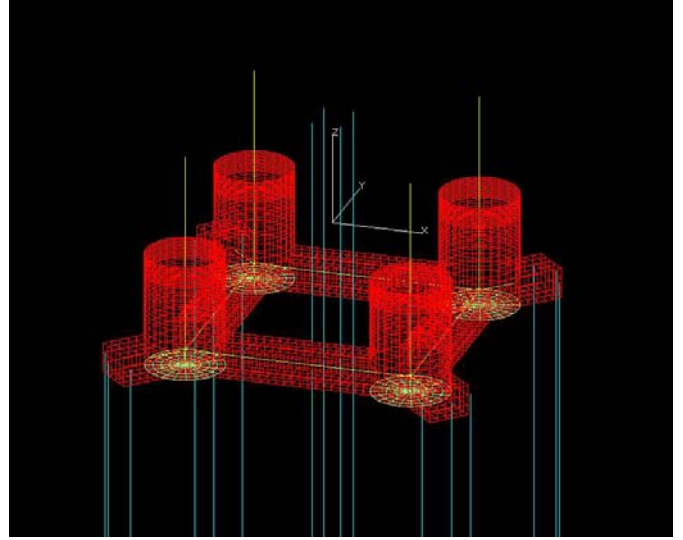


Fig. 4 Sample of Computer Model

## NUMERICAL MODEL

The uncoupled and fully coupled numerical model used compute the responses of the ETLP are based on the equations of motion described in Equations (1) and (2), respectively. A time domain solution is used to predict the six-degree-of-freedom rigid body motions, tendon and riser tensions and airgap. The potential flow hydrodynamic coefficients are found from the boundary integral technique described in [Lee, 1995]. The model includes Morrison members to account for viscous effect in the hull, tendons, and risers. Waves, wind, and current forces are generated for three hour simulations in both the un-coupled and fully coupled models. Fig. 4 shows a computer idealization of the model illustrating the panelized hull and the Morrison members.

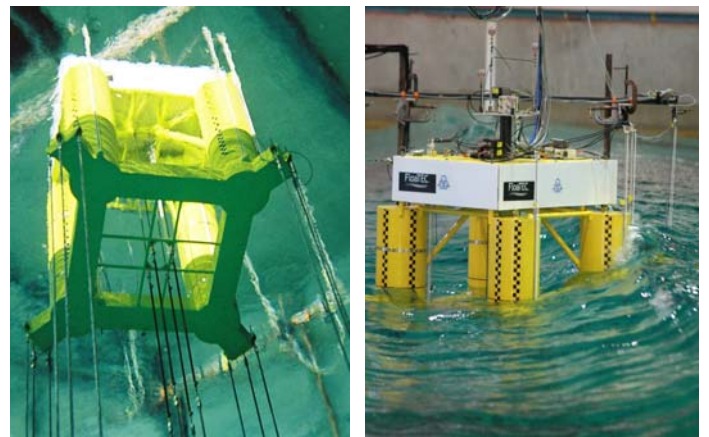


Fig. 5 Photos of Model Tests

The free surface panels also used to integrate the sum and difference frequency QTFs are not shown in Fig. 4.

**MODEL TESTS**

The model tests were carried out at the Offshore Technology Research Center (OTRC) in College, Station, Texas. The model was instrumented to measure six-degree-of-freedom global motion, airgap, and runup on the columns, tendon and riser tensions, and riser stroke. The prototype design contains 12 Top Tensioned Risers (TTRs) which were modeled as a group of four risers as illustrated in Fig. 2. Photographs of the model under test conditions are provided in Fig. 5. The model was subjected to an extensive test program in various combinations of wind, waves, and currents.

**FACILITY CALIBRATION**

Details of the environmental post-Katrina environmental conditions used in the analysis are provided in Table 2.

**Table 2 Post-Katrina 100-Year Hurricane Condition**

Waves		
Gamma	2.20	
Significant wave Height (m)	15.80	
Spectral Peak Period (s)	15.40	
Max wave Ht (m)	27.90	
Max crest Ht (m)	17.62	
Current Profile	Depth(m)	Velocity(m/s)
	0	1.80
	-38.00	1.35
	-76.00	0
	bottom	0
Wind	Speed	
1hour @ 10 m (m/s)	45.60	

Waves were calibrated without the model in the basin. Measurements were made at six locations using three calibration probes and three reference probes. The reference probes remain in position after the model was installed. The calibration probes were positioned at intended model location. A sample of the wave spectrum measured at one of the calibration probes is provided in Fig. 6.

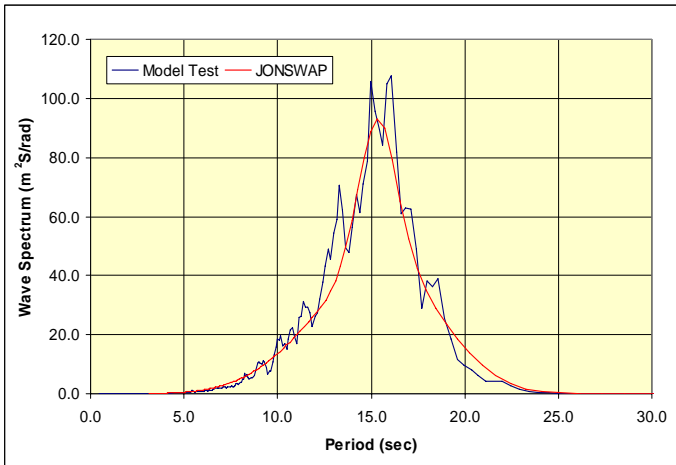


**Fig. 6 Sample of Target and Modeled Wave Spectrum**

Fig. 7 is a ranked plot comparing the wave heights and wave crests from the sequence of waves in the time series corresponding to the spectrum measure in the wave basin. The ranked plot is generated by

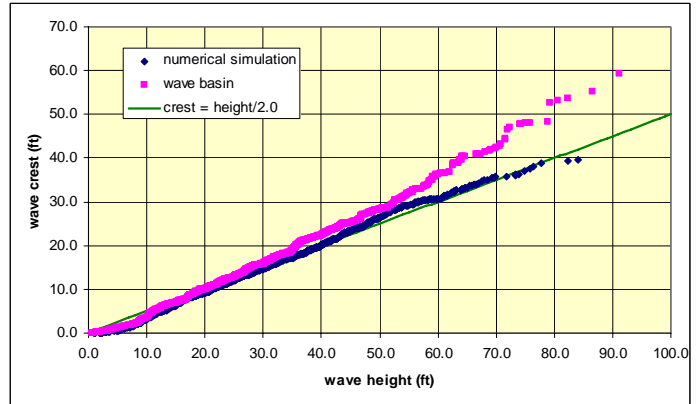


**Fig. 7 Wave Crest vs Wave Height**

performing a zero-crossing analysis on the waves identifying the crest heights and the wave heights. The respective data sets are ranked in ascending order and plotted against each other. This method assumes that the largest crest height occurs in the largest wave. The Figure also compares the crest heights of the waves generated in the wave basin to the crest heights simulated from a linear summation.

The results show that the heights of the crests from the wave basin are higher than the simulated crests, particularly in the higher waves. Also, the maximum crest height is not attained in the numerical simulation. This is a limitation of the numerical wave simulation.

**Dynamic Wind Force**

The dynamic wind force was applied using a line attached to a feedback controlled servo-winch. The line was fixed to the ETLP at the elevation of the center of pressure. The dynamic wind force drive signals were calibrated based on the wind force spectra and target RMS values measured in the wind tunnel tests. A comparison of the target and modeled spectrum for the 100-Year condition is shown in Fig. 8.

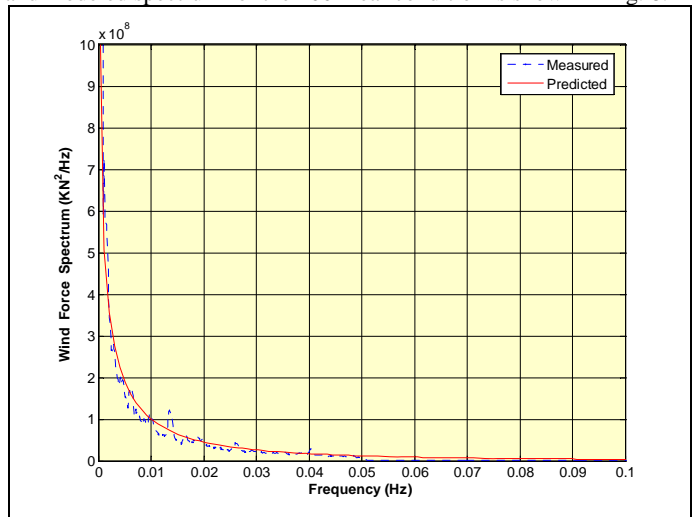


**Fig. 8 Sample of Target and Modeled Wind Spectrum**

**Current and SCR Forces**

The mean current force was applied using a weight over a pulley. The current force was combined with the steel catenary riser (SCR) force and applied at the same elevation.

# COMPARISON OF NUMERICAL SIMULATIONS AND MODEL TESTS

## Static Offset Tests

The model test setup is first evaluated by static offset tests to compare the predicted and measured restoring forces and hull setdown as a function of offset. Results of these tests are compared to the numerical predictions from the fully coupled and uncoupled models in Fig. 9~10.

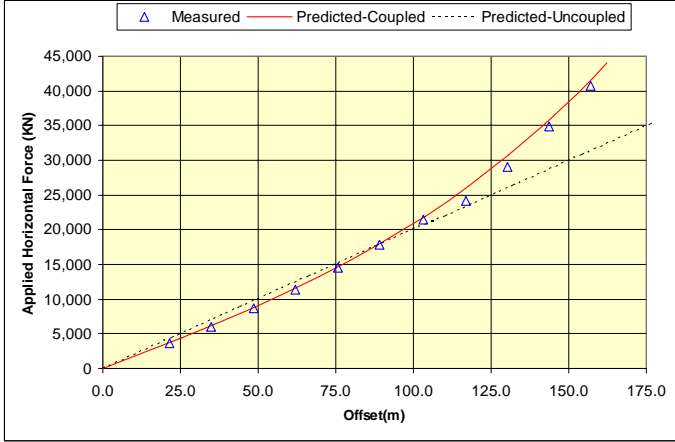


**Fig. 9 Predicted and Measured Offset vs Restoring Force**

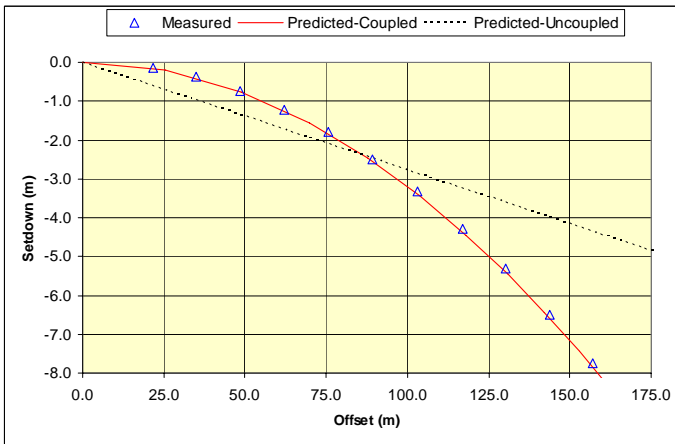


**Fig. 10 Predicted and Measured Offset vs Setdown**

These results show very good agreement between the fully-coupled predictions and the measure model results for both the setdown and the offset restoring forces. The uncoupled predictions are linear for the full range of offsets. Reasonable agreement between the uncoupled predictions and the measured restoring results is shown for offset up to approximately 350 ft. Uncoupled predictions of the setdown are generally over-predicted at offsets less than approximately 300 ft and under-predicted at offsets greater than 300 ft.

Fig. 11~12 show typical responses of the tendon and riser tensions, respectively, as a function of offset. Again, there is very good agreement between predictions from the fully coupled and measures tensions. The predicted tensions on both the tendons and the risers are highly nonlinear with respect to the offset. The tensions are under-

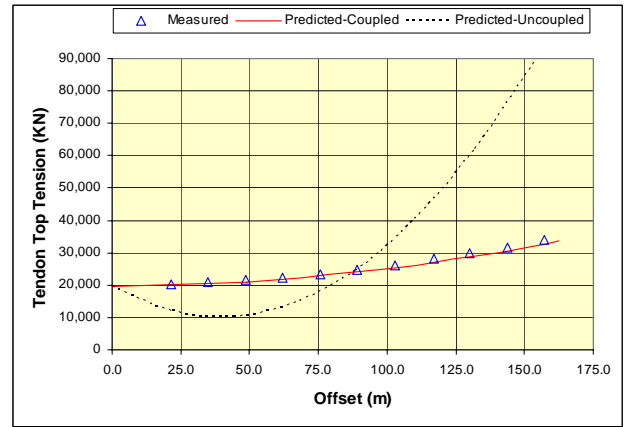


**Fig. 11 Predicted and Measured Offset vs Riser Tension**

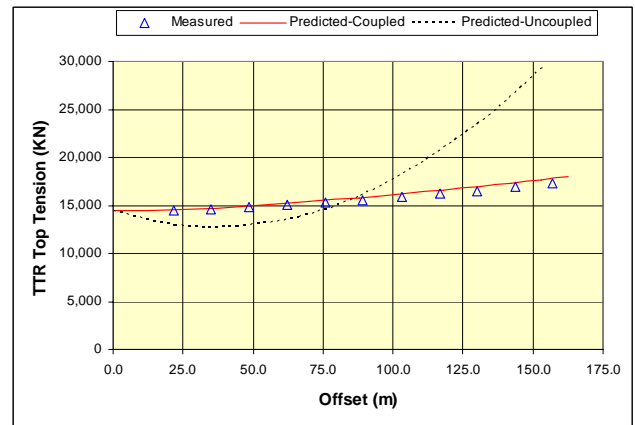


**Fig. 12 Predicted and Measured Offset vs Tendon Tension**

estimated for offsets less than 300 ft and over estimated for offsets greater than 300 ft.

## Comparison of Response Amplitude Operators

Following the static offset tests, the model setup was subjected to white noise spectra to measure the Response Amplitude Operators (RAOs). The measured RAOs are compared to the predicted frequency domain responses for surge, heave and pitch in Fig. 13~15, respectively. The white noise wave spectra were generated at a significant wave height of 20 ft as indicated in the figure. In general, good agreement was found at the lower periods for all three RAOs. The computed surge RAO tends to over-predict the surge response at the higher periods. This is due to viscous effects that are not accounted for in the frequency domain model.

A similar trend appears in comparison of the heave RAO. Also, the cancellation point in the predicted RAO approaches zero at approximately 15.4 sec. This is the point where the forces on the column cancel the forces on the pontoons but in the numerical model, does not account for the viscous effects. When the nonlinear damping is included, a non-zero response occurs at the cancellation periods. These occur because a drag force exists at all periods even when the inertia forces on the columns and pontoons cancel.

## Comparison of Fully-Coupled and Un-Coupled Responses

Time domain solutions from the coupled and uncoupled models are,

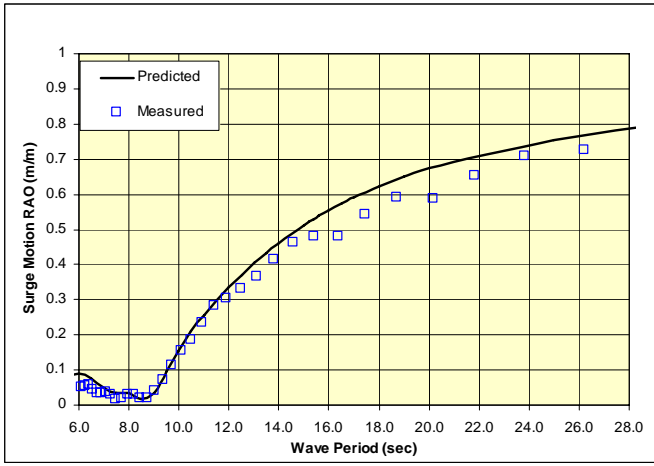


Fig. 13 Comparison of Surge RAOs

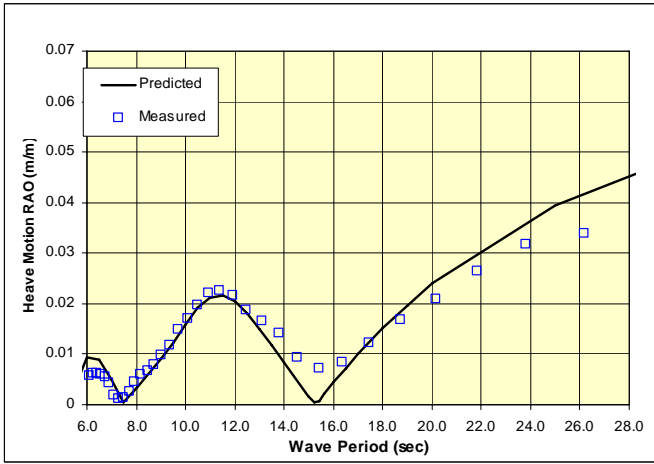


Fig. 14 Comparison of Heave RAOs

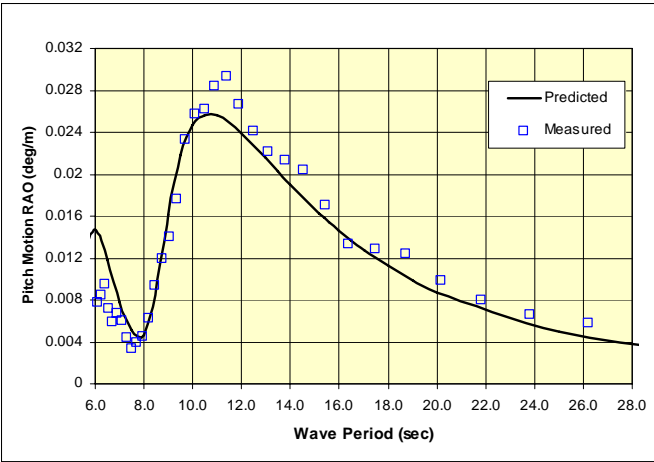


Fig. 15 Comparison of Pitch RAOs

compared to model test data for hull motions, tendon and riser tensions and airgap measurements. All comparisons are made for the 135-deg incidence heading. Fig. 16 compares the maximum offset (as a percentage of water depth), minimum heave, and minimum airgap. The maximum offsets at approximately 350 ft (approximately 7% of water depth) show good agreement among the coupled, uncoupled, and model test data. There is also very good agreement among all three data sets

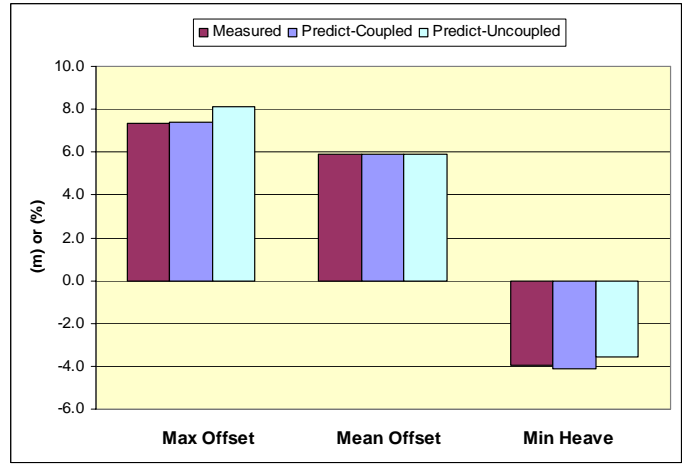


Fig. 16 ETLP Motion Statistics

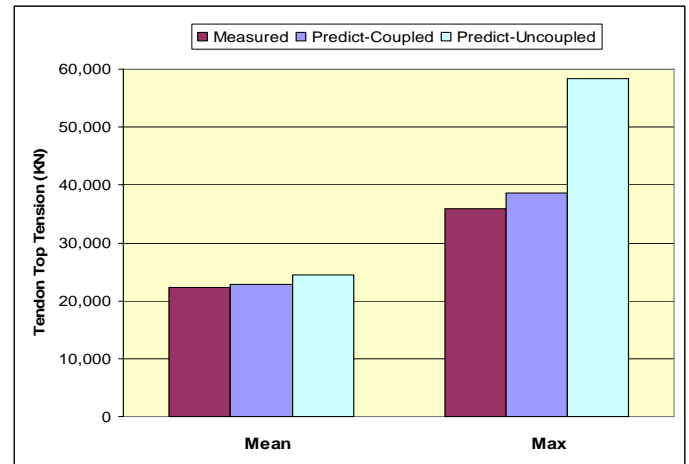


Fig. 17 Comparison of Tendon Tension

for the mean offset at 300 ft (approximately 6 % of the water depth). This is expected since the horizontal restoring force, as illustrated in Fig. 9, is approximately equal at these offset ranges. There is good agreement between the model test measurements and the fully couple model for minimum heave and minimum airgap. The heave is related mainly to setdown. Since the uncoupled model under predicts the setdown at this offset, as shown in Fig. 10, it is expected that the minimum heave is also under-predicted.

**Air Gap and Runup Analysis Using Ranked Plots**

The ranked plots are used to examine the airgap. Fig. 19 shows a ranked plot of the airgaps for the ETLP. The airgaps and crest heights are ranked in ascending order and plotted against each other. These plots show a high correlation between the airgaps and the crest heights even with the nonlinear crests in the measured waves. Although the maximum crest height is not achieved in the numerical simulations, the plot can be used to extrapolate to the maximum wave crest height and estimate the air gap.

Fig. 20 shows a ranked plot of the runup on two columns indicated in the figure. The plot compares the waves calibrated in the wave basin to the measurements. These plot exhibit more nonlinear effects of the column on the wave.

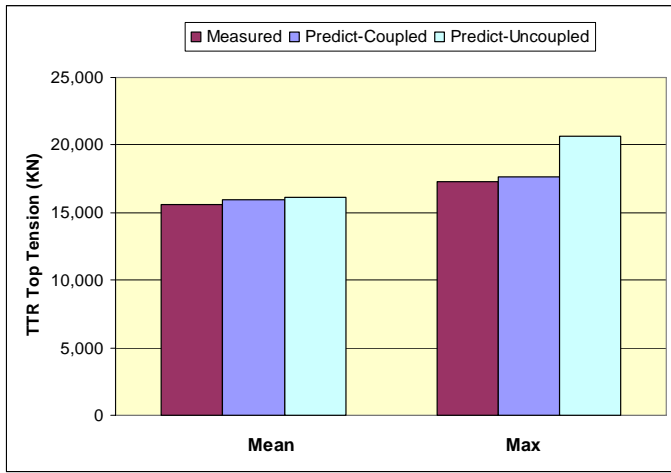


Fig. 18 Top Tensioned Riser Tension

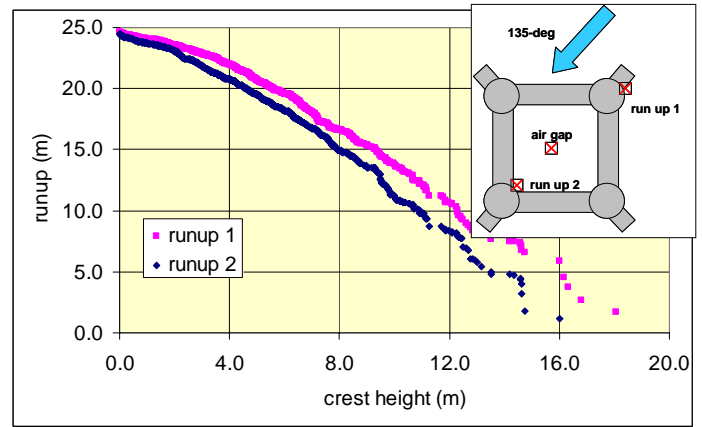


Fig. 20 Ranked Plot of Runup

- Setdown and consequently heave and airgap in the extreme offsets show poor agreement in the uncoupled model but very good agreement between the model tests and predictions from the fullycoupled model.
- The riser and tendon tension predictions by the uncoupled model show poor agreement with the model test data. Again is because coupling effects of the offset restoring force are not included in the model. Very good agreement is found between the fully coupled and model test measurements.
- Ranked plots showed a high correlation between wave crest heights and the airgap measures in the center of the model. Wave runup and airgap measured at or near the columns exhibited more non-linear relationship with the crest heights due to the presence of the columns.

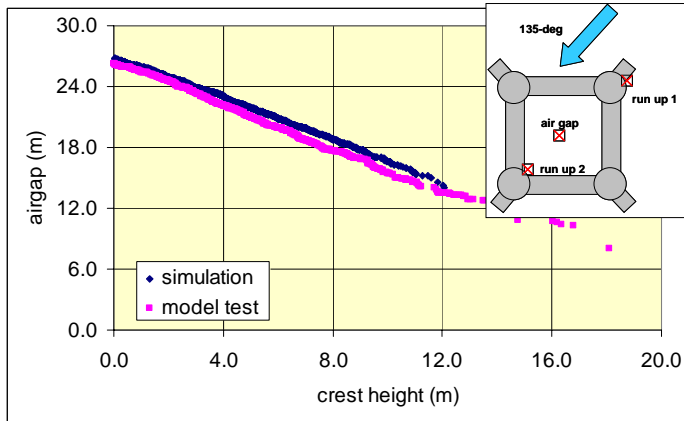


Fig. 19 Ranked Plot of Airgap

## SUMMARY AND CONCLUSIONS

This paper compares the results of numerical simulations to the measurements from a 1:92 scale model of an ETLP designed for the Gulf of Mexico in the post-Katrina environment. The numerical simulations include predictions from both uncoupled and fully coupled models. The following conclusions are based on the comparison:

- The ETLP design meets all criteria for the intact condition in the 100-Year Hurricane post-Katrina condition.
- In general, there is good agreement between the frequency domain predictions of the RAOs and the measured responses. In surge, viscous drag effects are apparent in longer wave periods, and the frequency domain tends to over predict the response. Viscous effects are also apparent in the model test heave data, which shows a nonzero response at the cancellation point and lower response at the longer periods.
- There is generally poor agreement between predictions of the uncoupled model and the model test measurements for extreme responses. This is attributed mainly to the tendon and riser restoring forces at the extreme offsets. Very good agreement was found between the fully coupled simulations and the model test measurements.

## ACKNOWLEDGEMENTS

The authors wish to thank FloaTEC, LLC for the model test data used in this paper.

## REFERENCES

- API, 2007, "Interim Guidance on Hurricane Conditions in the Gulf of Mexico", Bulletin 2INT-MET.
- Garrett, D.L., 1982, "Dynamic Analysis of Slender Rods", Journal Energy Resources Technology 104, pp.302-307.
- Kim, C.H., Kim, M.H., Liu, Y.H., Zhao, C.T., 1994, "Time Domain Simulation of Nonlinear Response of a Coupled TLP System", International Journal of Offshore and Polar Engineering 4, 281-291.
- Lee, C.H., 1995, 1995, "WAMIT Theory Manual", Department of Ocean Engineering, MIT, MA.
- Oran, Cenap, 1983, "Overall Dyanmic Characteristics of Tension Leg Platforms", Proceedings of OTC'83, OTC 4640, pp.507-516.
- Patel, M.H., 1983, "Dynamics of Offshore Structure", Butterworths, pp.312-315.
- Ran, Z., Kim, M.H., 1997, "Nonlinear Coupled Responses of a tethered Spar Platform in Waves", International Journal of Offshore and Polar Engineering 7, pp. 111-118.